A.C. conductivity, Dielectric and Electric Modulus Studies of $Li_4Ti_5O_{12}$ Anode films grown by RF Magnetron Sputtering

K. Hari Prasad [1], P. Muralidharan [2], E.S. Srinadhu [3], N. Satyanarayana [1,*]

[1]Department of Physics, Pondicherry University, Puducherry-605 014, India.
[2]Department of Chemistry, Rajiv Gandhi College of Engineering & Technology, Pondicherry 607402, India.
[3]Department of Physics & Astronomy, Clemson University, Clemson, South Carolina (SC) 29634, USA.
[*]Corresponding author. Tel: 0413-2654404; E-mail: nallanis2011@gmail.com

ABSTRACT

$Li_4Ti_5O_{12}$ (LTO) thin films were deposited at ambient temperature on Ti/silicon (Si) (100) substrate by using RF magnetron sputtering method. All the deposited thin-films were annealed at three different temperatures 400, 500 and 600 ^oC under an oxygen atmosphere to enhance the crystallinity. X-ray diffraction patterns showed the formation of cubic spinel structure phase of LTO thin film annealed at 600 ^oC. AFM micrographs for LTO thin films reveal the surface morphology and roughness modifications. The ac conductivity, dielectric constant (ε′) and electric modulus (M") for the as-deposited and post-annealed LTO thin films were evaluated by analyzing the measured impedance data as a function temperature in the frequency range of 100 Hz to 10 MHz.

Keywords: $Li_4Ti_5O_{12}$ thin films; RF magnetron sputtering; ac conductivity; dielectric constant; electric modulus.

1. INTRODUCTION

During the past decade, development of microelectronic mechanical systems, smart cards, on-chip power sources, portable electronic, etc., devices have been increased tremendously. To power these devices, all-solid-state thin film batteries are widely applied [1-9]. There have been only a few reports on the preparation of thin film node materials for lithium-ion batteries [10-16]. Li metal is the mostly used anode material for solid micro-batteries. However, the use of extremely reactive metallic lithium anode requires an expensive packaging technology. Moreover, pure lithium is highly volatile and melts at about 181 °C, a temperature usually lower than that applied during reflow soldering processes, widely used in the electronic industry.

$Li_4Ti_5O_{12}$, on the other hand, is an attractive alternative anode material and has many advantages such as reliable safety characteristics, negligible volume changes during cycling, no formation of a solid electrolyte interface, etc [10,11]. Many techniques such as sol–gel [12], spray pyrolysis [13], aerosol [14] radio-frequency magnetron sputtering (RFMS) [15] and pulsed laser deposition [16] techniques, etc., have been used for the fabrication of thin film electrodes. Among them, RF magnetron sputtering deposition is the most versatile technique for the fabrication of thin films, which offers precise control over film thickness, higher sputter rates at lower Ar pressures and less deviation from the target stoichiometric composition. Therefore, in the present work RFMS technique to deposit $Li_4Ti_5O_{12}$ thin films.

In this investigation, spinel LTO thin films were deposited on Ti/(100) oriented silicon (Si) substrate by RF magnetron sputtering technique. All the prepared LTO thin films were characterized using XRD, and AFM techniques. Also, the ac conductivity dielectric constant (ε′) and electric modulus (M") were evaluated by analyzing the measured impedance data using the winfit software for LTO thin films of as-deposited and post-annealed at different temperatures as a function of frequencies.

2. EXPERIMENTAL TECHNIQUES

2.1 Preparation of $LiCoO_2$ thin films

High purity (99.99%) spinel LTO target (50.88 mm diameter and thickness of 3 mm) bonded with the copper backing plate, the (100) oriented silicon (Si) substrate of thickness 0.125 mm were obtained from Testbourne Pvt. Ltd., USA. Initially, Si substrates were cleaned in the ultrasonic bath using solvents pure acetone, isopropanol and deionized water for 15 min., respectively and dried under a nitrogen atmosphere. As obtained LTO target was fixed to the magnetron, and Si substrate was fixed at 15 cm distance from the LTO target. A turbo molecular and rotary, as the backup, pumps were used to obtain the chamber base pressure of 1×10^{-7} Torr and then passed ultra-high pure Ar gas into the chamber through mass flow controller. The pre-sputtering process was performed for about 15 min. to remove surface contamination on LTO target and on Si substrate. Prior to the deposition of cathode materials, a thin titanium (Ti) film of ~ 25 nm was sputtered onto Si substrate to serve as an adhesive layer. LTO thin films were deposited on Ti/ (100) oriented silicon (Si) substrates by using RFMS power of 100 W at room temperature under an argon atmosphere at 1×10^{-3} Torr pressure. The thickness of the deposited LTO thin films measured using a quartz crystal thickness monitor was found to be 100 nm. The as-deposited LTO films were annealed at different temperatures 400, 500 and 600 ^oC in a pure oxygen atmosphere. Table 1 represents the sputtering deposition

conditions for the LTO thin films deposited on the Ti/(100) oriented Si substrate by using RFMS technique.

Table 1. Summary of sputtering parameters for the grown LTO thin films.

Target	:	$Li_4Ti_5O_{12}$ (2″ dia x 4mm thick)
Target to substrate distance	:	15 cm
Base pressure	:	$1x10^{-7}$ Torr
Working pressure	:	$1x10^{-3}$ Torr
Substrate temperature	:	None
RF power	:	100 W
Process gas	:	Ar (10 sccm)
Post-annealing temperature	:	400 °C, 500 °C and 600 °C
Duration of deposition	:	3 hrs
Substrate rotation	:	60 rpm
Substrate bias voltage	:	No bias voltage
Substrate	:	Ti/(100) oriented Si wafer
Thin film thickness	:	10000 A°

2.2 CHARACTERIZATION

XRD patterns of LTO films were recorded using the PANalytical, Philips, X' Pert Pro X-ray diffractometer having monochromatic X-ray source of CuK_α radiation with a wavelength (λ) of 1·541060 Å, operated at 40 kV and 30mA. The surface morphology of films was examined using atomic force microscopy (AFM) (NanoScope-V Multimode™ SPM, Veeco Instruments). Atomic Force Microscopy (AFM) images of the LTO films were recorded using the NanoScope -V Multimode™ SPM, Veeco Instruments. The AFM was operated in tapping mode (non-contact) to prevent the damage to the films and also to provide optimal image and quality data. From the 3-D AFM micrographs of the LTO thin films, grain shape, size and surface roughness parameters like root mean square (RMS) roughness (R_q), average surface roughness (R_a) are determined using Nanoscope analysis software. The impedance measurements were made using the following configuration

(Cu)/($Li_4Ti_5O_{12}$/Ti/(100) oriented Si)/(Cu)

for the as-deposited and post-annealed LTO thin film samples at different temperatures in the frequency range from 100 Hz to 10 MHz using Alpha A high-performance frequency analyzer of Novocontrol, Germany. The measured impedance data and the dimensions of LTO thin films were used for calculating AC conductivity (σ_{ac}), dielectric permittivity (ε'), and electric modulus (M") of LTO thin films.

3. RESULT AND DISCUSSION

3.1 XRD

Fig.1 shows the XRD patterns of as-deposited and post-annealed at 300, 400 and 500 °C LMO thin films rf-sputtered on Ti/Si (100) substrate alongwith the standard JCPDS data. From fig. 1, it is observed that as-deposited film exhibited, except one small peak at 2θ = 38.20°, peaks free XRD patterns, which confirm the formation of amorphous phase of LMO thin film. The observed small XRD peak at 2θ = 38.20° corresponding to the reflection from (002) plane of the pristine phase of Ti/Si (100) orientation film. From fig. 1, for the annealed at 400 °C of LTO thin film, new XRD peaks are observed at 2θ = 18.40°, and 43.30°. The intensity of the XRD peaks increases with the increase of annealing temperature up to 600 °C. From fig.1, the LTO thin film annealed at 600 °C showed the most prominent XRD peak at 2θ = 43.30°, which corresponds to the reflection from (400) plane. Apart from this, four other observed XRD peaks at 2θ = 18.40°, 35.5°, 47.40°, and 57.20° are compared with the JCPDS (card no. 49-0207) data and respectively assigned to the reflections from (111), (311), (331) and (333) planes, which confirm the formation of crystalline cubic spinel $Li_4Ti_5O_{12}$ phase.

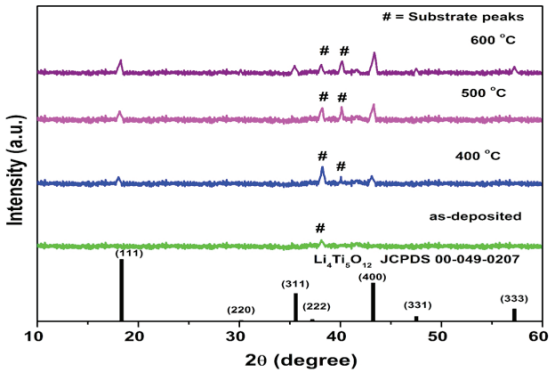

Fig. 1. X-ray diffraction patterns of as deposited and annealed at various temperatures of LTO thin films along with the standard JCPDS data

3.2 AFM

From fig. 2. [a, b, c, d]], the AFM images clearly show that the grain size increases with post-annealing temperature. From fig. 2 [a], the 3D AFM image of the as-grown LTO film shows smaller individual grain with low roughness. From fig. 2. [b, c, and d] 3D AFM micrographs of the post-annealed (at 400 °C, 500 °C, and 600 °C) LTO thin films show denser granular structure, and it is also observed that there is a decrement in the separation between the grains and grain boundary increases with the increase of temperature. From the AFM images, the grain size, R_a, and R_q values were evaluated using Nanoscope analysis software and are presented in table 2. From table 2, it is observed that the grain sizes are found to be 37 nm, 49 nm, 85 nm, and 98 nm, respectively for the as-deposited and post-annealing temperatures at 400 °C, 500 °C and 600 °C of LTO films, which indicate that the grain size increases with increasing of post-annealing temperature [7]. The grain size plays an important role in the electrochemical performance of Li-ion batteries, because, the small grain size which can provide the large specific surface area, shorter Li-ion diffusion path and easy to migrate the Li-ions from the in and out of the spinel LTO system. From table 2, it is also found that the post-annealed at 600 °C of LTO film has the highest surface roughness (R_a: 18 nm and R_q: 16.6 nm) and the as-grown LTO thin film has the smallest surface roughness (R_a of 1.55 nm and R_q of 1.92 nm).

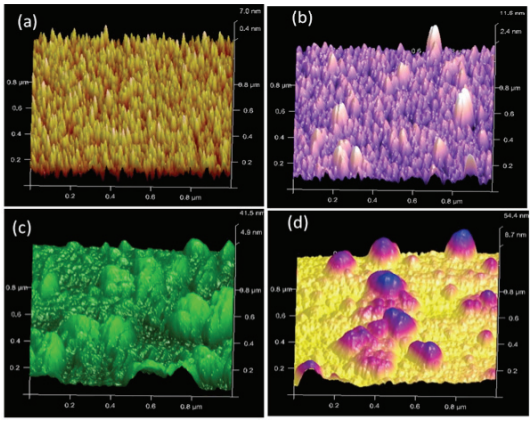

Fig. 2. 3-dimensional AFM surface micrographs of the $LiCoO_2$ thin films of **[a, b]** as-deposited, and post-annealed at **[c, d]** 400 ^oC, **[e, f]** 500 ^oC, and **[g, h]** 600 ^oC.

Table 2:

Temperature (^oC)	Average roughness (nm) R_a	RMS roughness (nm) R_q	AFM grain size (nm)
As-deposited	1.55	1.92	37
400 ^oC	2.14	2.78	49
500 ^oC	14	11	85
600 ^oC	18	16.6	98

3.3. AC conductivity (σ_{ac})

From fig. 3, the frequency dependent conductivity plots showed two distinct regions within the measured frequency window, (i) the low-frequency plateau region and (ii) high-frequency dispersion region. The plateau region corresponds to frequency independent conductivity $\sigma_{(0)}$ or dc conductivity (σ_{dc}) and it is evaluated by extrapolating the plateau region to the zero frequency (Y-axis). The frequency independent conductivity may be attributed to the long-range transport of free charge carriers with the applied field in LTO thin films. The observed a.c. conductivity in the high-frequency dispersion region follows Jonscher's universal power law (JUPL).

$$\sigma_{(\omega)} = \sigma_{(0)} + A\omega^s \qquad (1)$$

where $\sigma_{(\omega)}$ is the ac conductivity, $\sigma_{(0)}$ is the zero frequency limit of $\sigma_{(\omega)}$, A is a constant, and s is the power law exponent ($0 < s < 1$).

From fig.3, it can be observed that the frequency at which the dispersion region deviated from the plateau is defined as the hopping frequency (ω_p), where, the relaxation effects starts. Also, it can be observed that the hoping frequency moved towards the higher frequency with the increase of temperature in the LTO thin film , which may be due to hopping of electrons between adjacent sites, results in local displacement of charge carriers in the direction of the applied frequency. Hence, the observed dispersion region of conductivity curves may follow the diffusion controlled relaxation (DCR) model [17, 18].

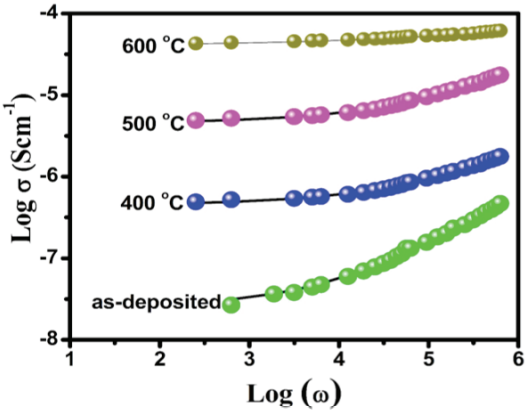

Fig. 3. Log (σ_{ac}) versus log(ω) plots obtained at room temperature of LTO thin films as-deposited and post- annealed at different temperatures.

3.4 Dielectric constant (ε')

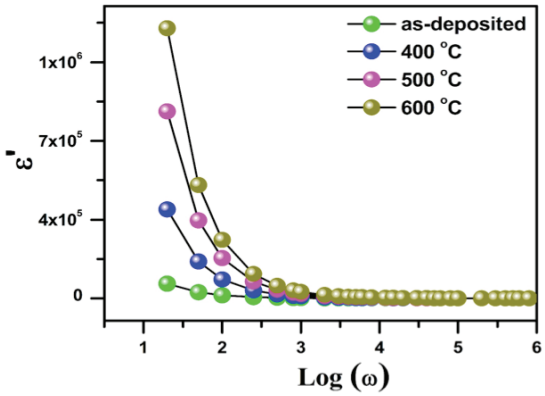

Fig. 4. Real part of dielectric constant (ε') versus log(ω) plots obtained at room temperature of LTO thin films as-deposited and post-annealed at different temperatures.

From fig. 4, it is observed that, with the increase of frequency, dielectric permittivity (ε') decreases and attains a constant value at high frequencies and it is also observed that the dielectric permittivity increases with the increase of temperature. From fig. 4, the observed dielectric permittivity (ε') at high frequencies may be attributed to the periodic reversal of the high electric field results in no charge accumulation at the interface and hence, the dielectric permittivity (ε') remain constant. The motion of the charge without accumulation can be explained in terms of the carrier's diffusion mechanism [17, 18]. From fig. 4, the increase of dielectric permittivity (ε') with a decrease of frequency can be attributed to the contribution of charge accumulation at the interface, which results the formation of space charge region at the electrode and electrolyte interface [17, 18]. This will hinder the motion of the mobile charge carriers in the sample and hence, the dielectric permittivity (ε') value increases with the decrease of frequency. From fig. 4, the increase of dielectric permittivity (ε') with increasing temperature may be due to the increase of thermal activation and local displacement of charge carriers, which may help to

TechConnect Briefs 2017, TechConnect.org, ISBN 978-0-9975117-9-6

increase the dielectric permittivity (ε') with the increase of temperature [17, 18].

3.5 Electric Modulus (M'')

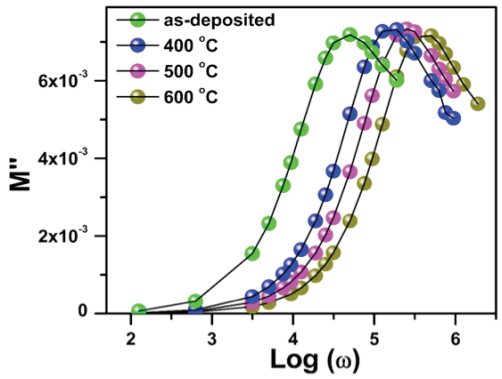

Fig. 5. Imaginary part of electric modulus (M'') versus log(ω) plots obtained at room temperature of LTO thin films as-deposited and post-annealed at different temperatures.

From fig. 5, the imaginary part of electric modulus (M'') versus log (ω) exhibit the peak at the relaxation frequency maximum (f_{max}) and its frequency position shifts towards higher frequency regions and it is also observed that the broadness of the electric modulus (M'') versus log (ω) curve increases with increase of temperature. The relaxation frequency maximum (f_{max}) peaks shift towards the higher frequency region with the increase of temperature, which can be attributed due to the variation of relaxation time (τ) of the charge carriers were found to exhibit non-Debye type behavior in the LTO thin film sample [17-18].

4. CONCLUSION

Nanocrystalline spinel $Li_4Ti_5O_{12}$ (LTO) thin films were grown at room temperature by RF magnetron sputtering on Ti/ (100) oriented silicon (Si) substrate and annealed at different temperatures up to 600 ^oC under an oxygen atmosphere. The phase purity of the LTO films was confirmed by X-ray diffraction result. The surface morphology and roughness of the LTO films were obtained from AFM results. AC conductivity (σ_{ac}) and dielectric constant (ε′) increased with a rise in the annealing temperatures of LTO thin films. The imaginary part of the electric modulus (M'') studies were revealed the non-Debye nature behavior of LTO thin films.

ACKNOWLEDGMENT

NS would like to thank the DST-Nano mission, Govt. of India, for providing grants in the form of research project sanction letter No.: SR/S5/NS-49/2005 dated on 30-07-2010 and NRB-DRDO, Govt. of India, for providing grants in the form of research project sanction letter No.: NRB-377/MAT/16-17, dated on 19-04-2016, for developing five targets DC/RF magnetron sputtering facility for developing all solid state thin film lithium ion micro-batteries. Authors thank CIF, Pondicherry University, for extending the experimental facilities.

REFERENCES

[1] J. M. Tarascon, M. Armand, Nature, 414 (2001) 359-367.
[2] M. M. Thackeray, W. I. F. David, P. G. Bruce, J. B. Goodenough, Mater. Res. Bull., 18 (1983) 461-472.
[3] D. K. Kim, P. Muralidharan, H. W. Lee, R. Ruffo, Y. Yang, C. K. Chan, H. Peng, R. A. Huggins, Y. Cui, Nano Lett., 8 (11) (2008) 3948-3952.
[4] J. Feng, X. Gao, L. Cia, S. Xiong, RSC Adv., 6 (2016) 7224-7228.
[5] J. Wang, Y. Li, X. Sun, Nano Energy, 2 (2013) 443-467.
[6] K. Hari Prasad, N. Naresh, N. Satyanarayana, Material Today: Proceedings 3 (10) (2016) 4040-4045.
[7] K. Hari Prasad, S. Vinoth, N. Satyanarayana, Material Today: Proceedings 3 (10) (2016) 4046-4051.
[8] K. Hari Prasad, A. Ratnakar, N. Satyanarayana, Material Today: Proceedings 3 (10) (2016) 4064-4069.
[9] L. Baggetto, R.A.H. Niessen, F. Roozeboom, P.H.L. Notten, Adv. Funct. Mater. 18 (2008) 1057.
[10] T. Ohzuku, A. Ueda, N. Yamamoto, J. Electrochem. Soc. 142 (1995) 1431.
[11] T.F. Yi, L.J. Jiang, J. Shu, C.B. Yue, R.S. Zhu, H.B. Qiao, J. Phys. Chem. Solids 71 (2010) 1236.
[12] Y.H. Rho, K. Kanamura, M. Fujisaki, J. Hamagami, S. Suda, T. Umegaki, Solid State Ionics 151 (2002) 151.
[13] Y. Yu, J.L. Shui, C.H. Chen, Solid State Commun. 135 (2005) 485.
[14] R. Inada, K. Shibukawa, C. Masada, Y. Nakanishi, Y. Sakurai, J. Power Sources 253 (2014) 181.
[15] F. Wunde, F. Berkemeier, G. Schmitz, J. Power Sources 215 (2012) 109.
[16] Jianqiu Deng, Zhouguang Lu, I. Belharouak, K. Amine, C.Y. Chung, J. Power Sources 193 (2009) 816-821.
[17] P. Muralidharan, M. Venkateswarlu, N. Satyanarayana, Solid State Ionics, 166 (2004), 27-38.
[18] P. Muralidharan, N. Nallamuthu, I. Prakash, N. Satyanarayana, J. Am. Ceram. Soc., 90 (2007) 125-131.